Journal of Geophysical Research - Solid Earth

Supporting Information for

GPS Imaging of Mantle Flow-Driven Uplift of the Apennines, Italy

by

William C. Hammond[1] and Nicola D'Agostino[2]

1) Nevada Geodetic Laboratory
Nevada Bureau of Mines and Geology
University of Nevada, Reno
whammond@unr.edu

2) Istituto Nazionale di Geofisica e Vulcanologia
Osservatorio Nazionale Terremoti
Rome, Italy

Contents of this file

Additional Supporting Information (Files uploaded separately)

Supplementary Table S2 - GPS velocities and uncertainties

Supplementary Table S1 - Networks and internet sites from which we obtained RINEX data

Introduction

The supplementary materials provide detailed information about parts of the GPS data analysis. Specifically, the correction for glacial isostatic adjustment, the estimation of the spatial structure function that is needed for GPS Imaging, and resolution tests of the GPS Imaging of vertical velocity. A separate file contains supplementary Table S1. This table contains the GPS velocities which are the main product of the GPS data processing and MIDAS estimation and are the underlying data for the GPS Imaging analysis presented in the main text and figures.

Supplemental Materials

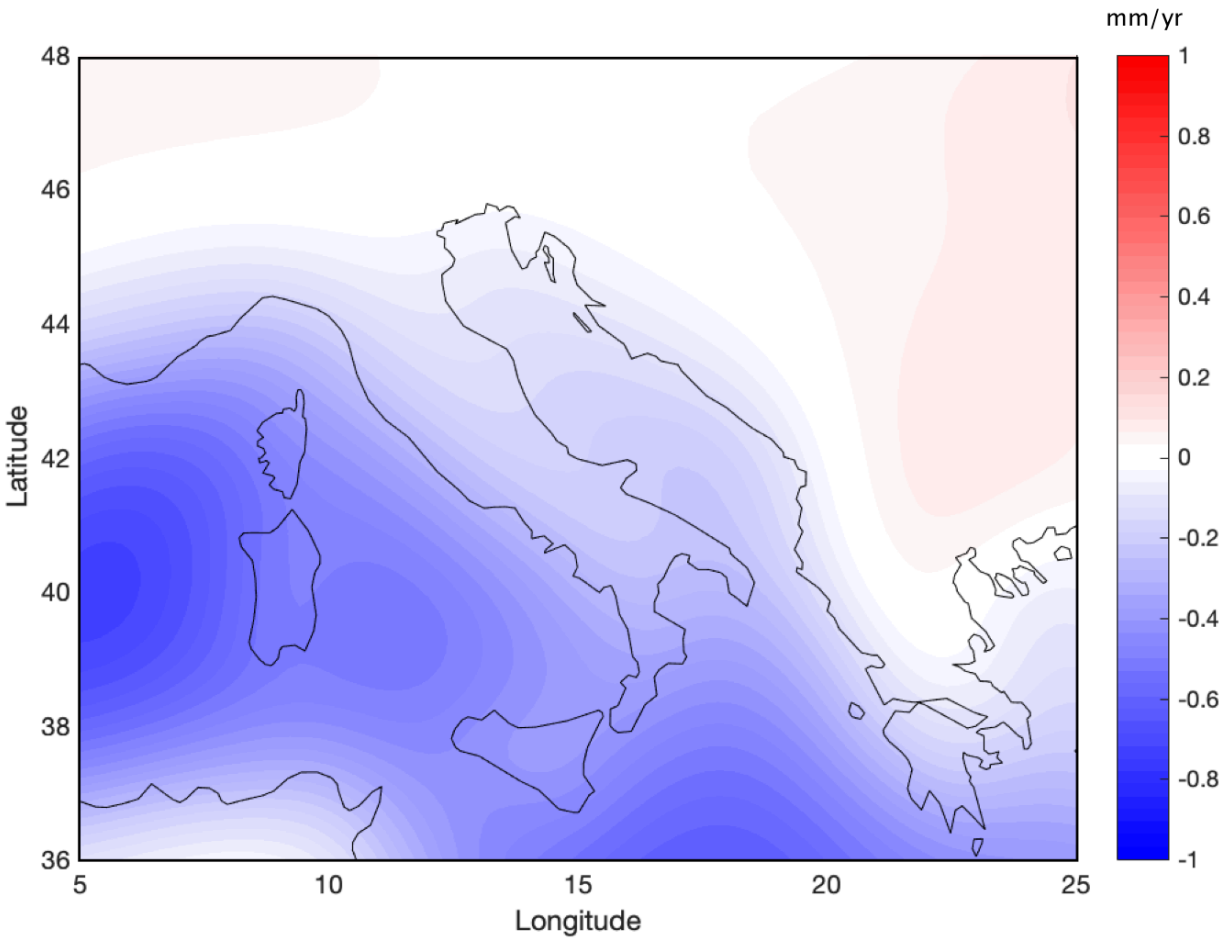

Supplementary Figure S1. Prediction of vertical geodetic velocity from ICE-6G model (Peltier et al., 2015, obtained from https://www.atmosp.physics.utoronto.ca/~peltier/data.php) used as a correction for vertical velocities estimated from GPS. Note color scale is different from that used in figures in main text in order to better highlight the gradients in vertical velocity. The scale in this figure extends from -1 mm/yr downward (blue) to +1 mm/yr upward (red).

Estimation of the Spatial Structure Function

We derive the spatial structure function (SSF) needed for the GPS Imaging analysis from the vertical GPS velocities as described in *Hammond et al.,* (2016). This function is a statistical representation of how the similarity in values between pairs of stations decreases with distance, analogous to a semivariogram in kriging analysis, but estimated using a robust approach that is itself insensitive to outliers in the vertical velocity data. In our implementation an SSF always has value 1 at zero distance and value zero at distance 180 degrees (the maximum distance on Earth's surface) decreasing monotonically. The SSF we derive from our GPS velocity dataset falls to 0.5 at ~0.3 degree, and to under 0.05 at 1 degree, and therefore falls off faster with

distance than the one obtained in Figure 4C of Hammond et al., (2016) for the California and Nevada region. This indicates that the horizontal length scales in the vertical rate field for the Italian Peninsula are on average shorter than those in California and Nevada. Supplementary Figure S1 illustrates the stages of the generation of the SSF, its caption describes the

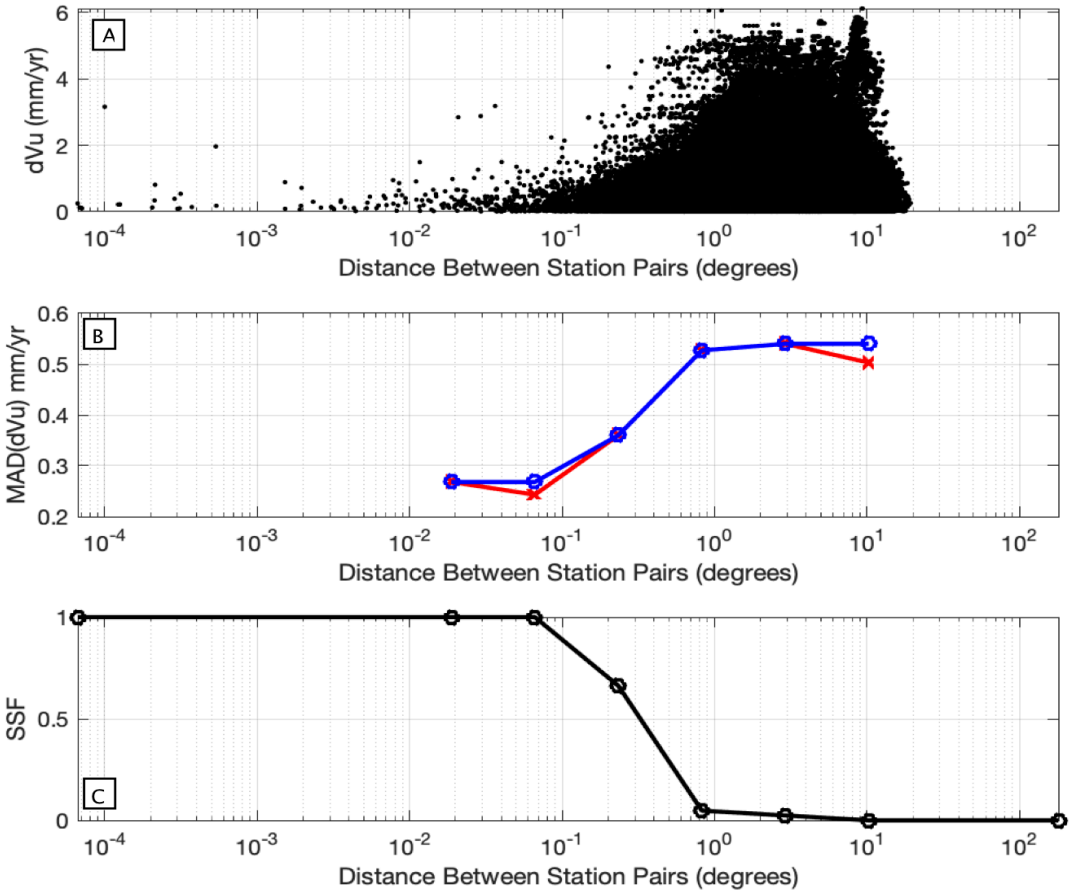

Supplementary Figure S2. Derivation of the SSF used in the GPS Imaging analysis. A) Scatterplot of the absolute value of the difference in median spatial filtered vertical GPS velocities as a function of distance between all pairs of stations within the domain shown in Figure 3. B) The median absolute deviation (MAD) of the differences in vertical velocity (red) for groups of rate differences inside bins centered at the data points indicated by 'x' and 'o' symbols. Larger values indicate greater spread of rates within the bin. Blue is the same curve except that the value at each point is the maximum of the red value and the previous value to enforce the SSF to be monotonically increasing. C) SSF function derived from the blue function (z) where SSF = (max(z) - z)/max(z) and then padded with a 1 at the beginning and a zero at the end.

Tests of Stability of GPS Imaging Vertical Rate Results

We assess the stability and repeatability of the GPS Imaging results by performing a sequence of tests using various subsets of the data. We divide the data into several different subsets and repeat the imaging using the same method used to generate Figure 3. Because some stations show significant variability in the vertical rates over multi-annual periods (e.g. Figure 10) the rates obtained may be sensitive to the time period over which they collect data, especially for stations with shorter durations between first and last observation.

In Figure S3 we show the results of dividing the data into three different time intervals. For each time interval we take the part of the GPS time series that lies within the indicated interval and use the station if the truncated time series is at least as long as the duration cutoff used in Figure 3 (2.5 years). The time intervals used are 2005.0 - 2012.0, 2008.0 - 2014.0, and 2012.0 - 2019.0. The first and last intervals are non-overlapping. We apply the MIDAS algorithm to the resulting truncated vertical component GPS time series to obtain the rates in each time period. Station coverage is not identical in all time periods owing to the installation or deactivation of some stations. A station can appear in more than one image if its time series is long enough to have at least 2.5 years in more than one time interval. While some details vary from image to image, the main features in the uplift signal, including uplift along the Apennines, Calabria and northern Sicily are present in all three images and have similar amplitudes. This indicates that the main features of the uplift and subsidence signals are not highly time variable. The greatest differences are in the Dinaric Alps east of the Adriatic Sea, where GPS station coverage is least complete.

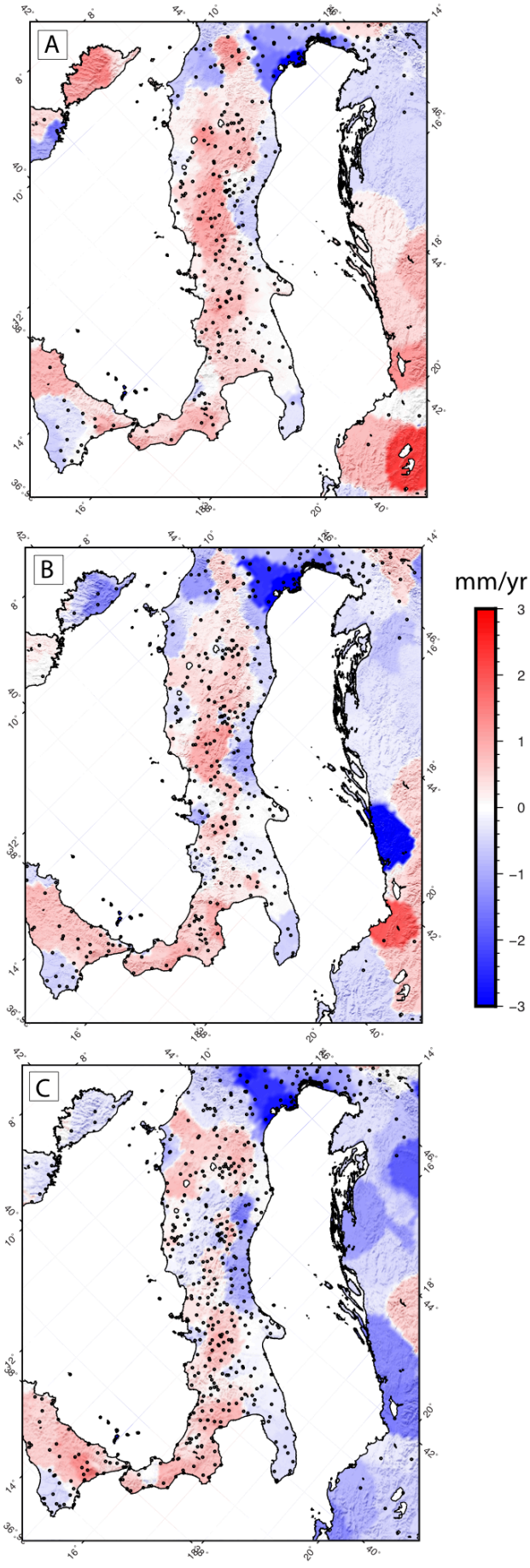

Supplementary Figure S3 (right). Results of GPS Imaging applied to time intervals of A) 2005.0 - 2012, B) 2008.0-2014.0, C) 2012.0 - 2019.0. Black dots are GPS stations inside the time interval that were used to perform the imaging.

We next show the results of dividing the data into two randomly selected non-intersecting subsets, where every station is in either one set or the other with no overlap. This selection tests whether the spatial coverage of GPS stations is redundant with respect to the signals of uplift we discuss. Selection of stations is done quasi-randomly by sorting stations by distance from the geometric center of the figure bounds, and then taking odd numbered stations as one set and even numbered stations as the other. This ensures that each subset has roughly the same number and same geographic coverage, and that differences in the imaging result are attributable to noise related to station coverage. The result, shown in Supplementary Figure S4, indicates that most of the long wavelength signal is consistent between the two figures, including along the length of the Apennines, Calabria and Sicily. Some minor differences are apparent, including in the central Apennines. The degree of difference between the two images based on the even/odd halves of the data is similar to the degree of difference between the separate time periods discussed in Supplementary Figure S3 above. This suggests that the spatial density of stations is approximately as important as the temporal duration of GPS coverage in the imaging. In each case using half the data provides an image that is approximately correct but is improved by including the addition of the other half. As in the test of different time periods the differences are greatest in the Dinaric Alps region where GPS station coverage is weaker.

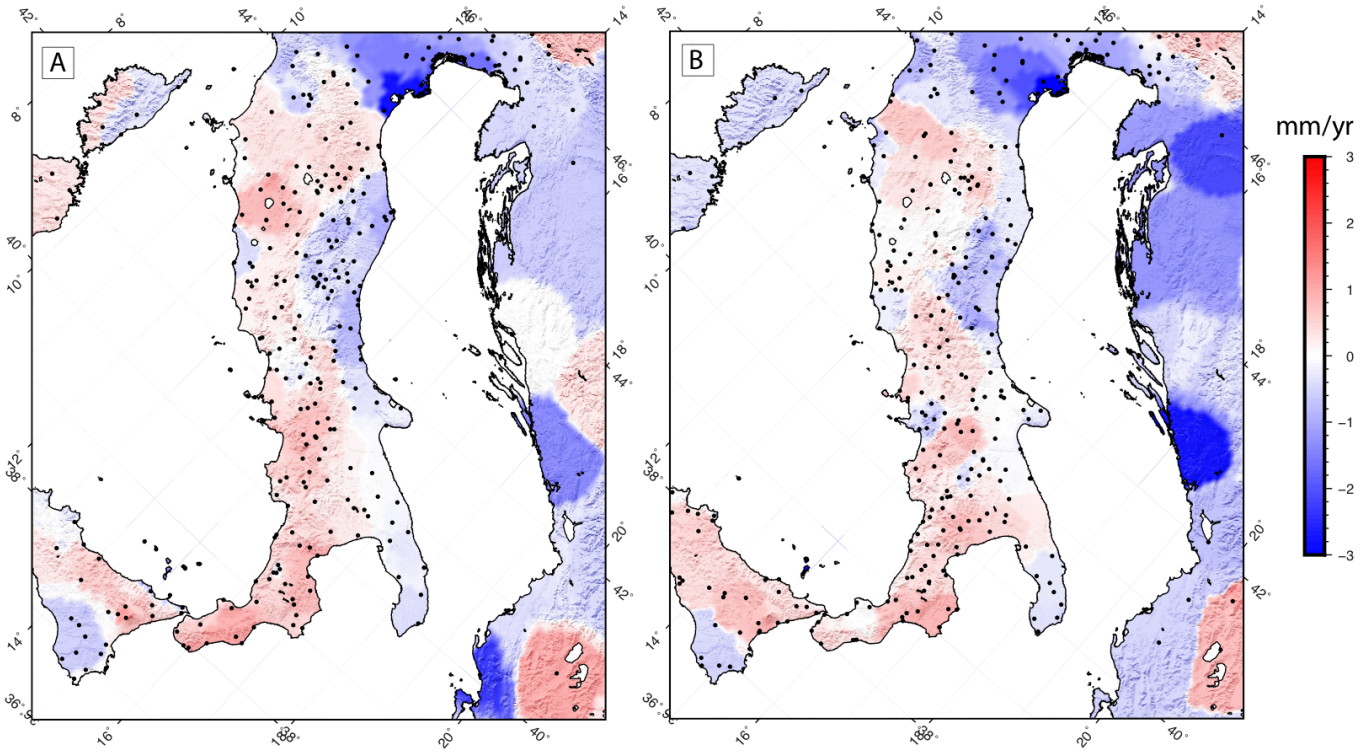

Supplementary Figure S4 (above). A) GPS Imaging of vertical rate using the even numbered stations when sorted by distance from the figure center. B) GPS Imaging usin the odd half of the stations.

Our third test varies the cutoff in minimum time series duration used for the imaging. Shorter duration time series are more prone to bias from multiannual vertical rate variability. Thus, we expect that imaging based on shorter duration time series to be less reliable owing to the interval sample bias, in addition to the higher aleatory uncertainty inherent to estimating trends from short time series. Since network coverage increases over time the inclusion of shorter time series could conceivably cause a temporal bias similar to the tests of different time series intervals detailed above. However, allowing shorter duration time series supplements the spatial coverage, and while they may introduce noise in the imaging, GPS Imaging exploits the power of numbers to find the median signal. This test illustrates the value of including shorter duration time series as opposed to restricting the analysis to only a sparser network of long-observing stations.

Supplementary Figure S5 shows the result in A) of imaging with only stations having 10 or more years of time series duration, and in B) the result of imaging using only stations with between 2.5 years and 10 years duration. The 10-year cutoff was chosen so that there are a similar number of stations in the two subsets, however these subsets to not have the same geographic distribution. The imaging results shows that for longer duration time series, the vertical rate field is similar to the field obtained using all the data (Figure 3), with uplift over nearly the entire length of the Apennines, Calabria and northern Sicily, though misses some of the uplift in the Larderello and Monte Amiata regions. The image obtained using only shorter duration time series has uplift in the northern Apennines and Calabria, but is missing uplift in the Central to Southern Apennines. This suggests that having a broad and dense distribution of GPS stations with long observation histories (>10 years data) is essential for resolving the signals of geographically coherent vertical uplift in the Apennines, but also it benefits substantially from the introduction of relatively new stations with shorter duration time series.

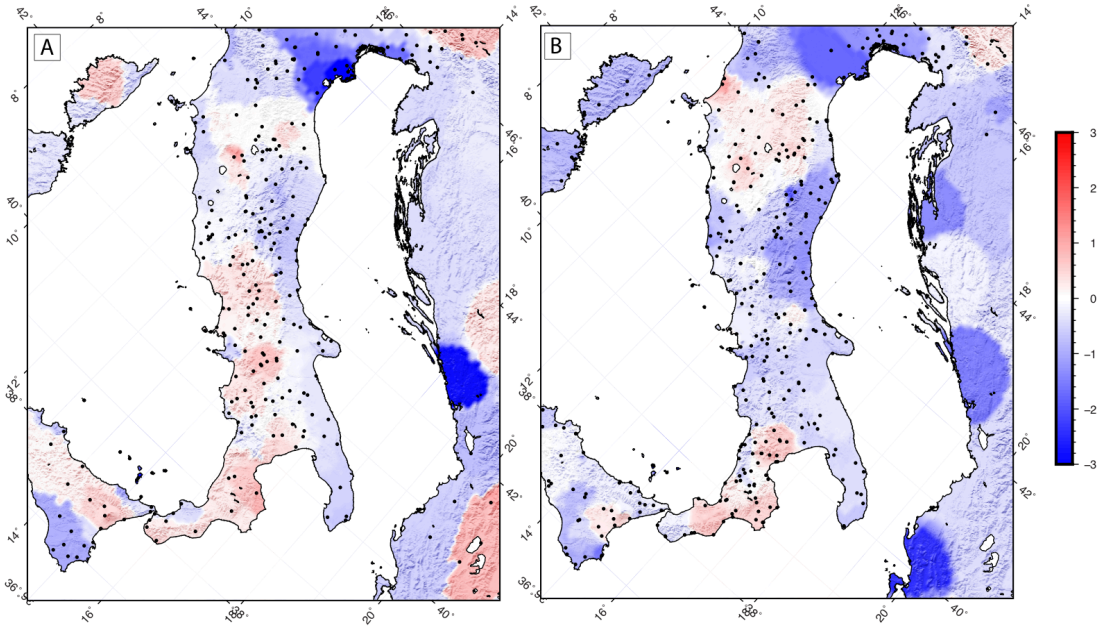

Supplementary Figure S5. GPS Imaging using A) only stations with 10 years or greater duration time series and B) only stations with between 2.5 and 10 years duration time series.

Regularization of strain rate

In our GPS Imaging of horizontal tensor strain rates described in the main text we estimate velocity gradients over a finite distance which we must choose a priori. The choice of horizontal strain length scale (w) has an effect on the degree of smoothness and misfit to the data. As in all strain mapping analyses, a longer length scale tends to create a smoother and simpler variation of estimated strain rate with a smaller overall model norm, greater data misfit, but greater certainty in individual strain rate estimates at grid points. In order to find a model with both low misfit and low uncertainty we perform our strain rate estimation using test values of w from 2 to 20 km, stepping at 2 km intervals. For each model we compute the mean and median of the weighted sum of residuals to represent misfit between the data and model predictions. To represent the model norm we calculate the root-sum-square of each strain rate component (dilatation, shear and magnitude of strain rates). Figure S6 shows the model misfit and norms as a function of w in km. The results show that model norms decrease and model misfits increase with increasing w. In the text we present a model with value of w = 8 km since this the rate of reduction in model norm begins to decrease substantially, and this value the model misfit begins to climb rapidly.

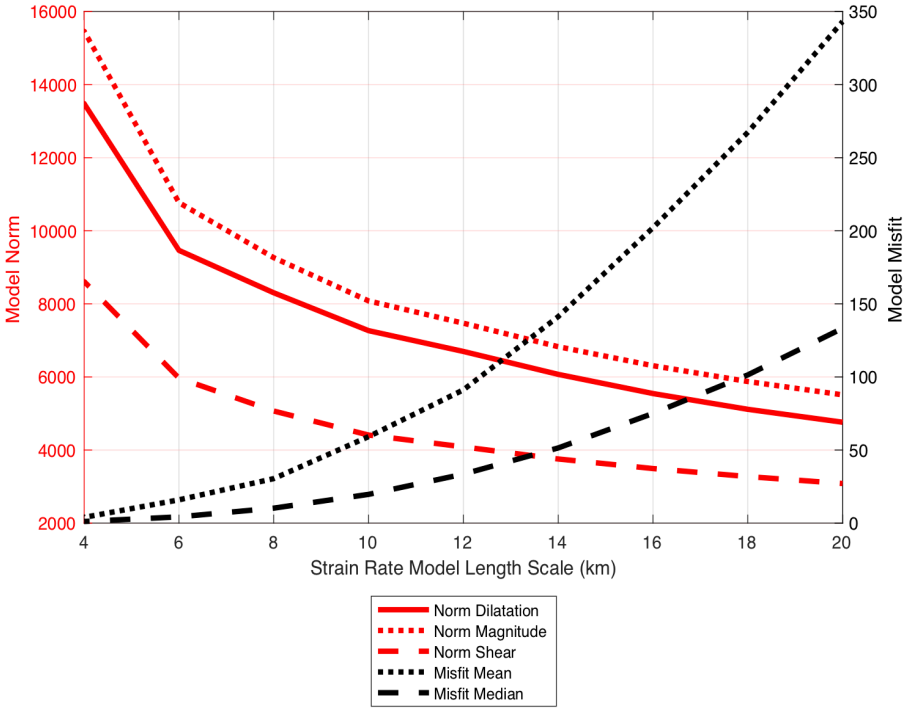

Supplemental Figure S6. Model misfit and model norm as a function of strain rate length scale parameter w in km.